LA-UR 96-0101

CONF-960415--2

Los Alamos National Laboratory is operated by the University of California for the United States Department of Energy under contract W-7405-ENG-36

TITLE VERIFICATION OF THE MCNP™ PERTURBATION TECHNIQUE

AUTHOR(S) Gregg W. McKinney
Jess L. Iverson

SUBMITTED TO American Nuclear Society 1996 Radiation Protection and Shielding Topical Meeting, April 21-25, 1996, No. Falmouth, Massachusetts

DISCLAIMER

Los Alamos Los Alamos National Laboratory
Los Alamos, New Mexico 87545

VERIFICATION OF THE MCNP™ PERTURBATION TECHNIQUE

Gregg W. McKinney and Jess L. Iverson
Los Alamos National Laboratory
XTM, MS B226
Los Alamos, NM 87545
(505)665-8367

ABSTRACT

The differential operator perturbation technique has been incorporated into the Monte Carlo N-Particle transport code MCNP and will become a standard feature of future releases. This feature includes first and second order terms of the Taylor series expansion for response perturbations related to cross-section data (i.e., density, composition, etc.). Perturbation and sensitivity analyses can benefit from this technique in that predicted changes in one or more tally responses may be obtained for multiple perturbations in a single run. The user interface is intuitive, yet flexible enough to allow for changes in a specific microscopic cross-section over a specified energy range. With this technique, a precise estimate of a small change in response is easily obtained, even when the standard deviation of the unperturbed tally is greater than the change. Furthermore, results presented in this report demonstrate that first and second order terms can offer acceptable accuracy, to within a few percent, for up to 20-30% changes in a response.

I. INTRODUCTION

Over the last few decades, users of the Monte Carlo radiation transport code MCNP[1] have expressed the need for a perturbation capability. The perturbation technique chosen for inclusion as a standard feature in future releases of MCNP is described in this paper. This new MCNP feature will provide the radiation transport analyst with a powerful tool for predicting the effect of multiple perturbations within a single run.

The evaluation of response sensitivities to cross-section data involves finding the ratio of the change in response to the infinitesimal change in the data, as given by the Taylor series expansion. In deterministic methods, this ratio is approximated by performing two calculations, one with the original data and one with the perturbed data. This approach is useful even when the magnitude of the perturbation becomes very small. In Monte Carlo methods, however, this approach fails as the magnitude of the perturbation becomes small, due to the uncertainty associated with the response. For this reason, the differential operator technique was developed.

The differential operator perturbation technique as applied to the Monte Carlo method was introduced by Olhoeft[2] in the early 1960's. Nearly a decade after its introduction, this technique was applied to geometric perturbations by Takahashi.[3] A decade later, the method was generalized for perturbations in cross-section data by Hall[4,5] and later Rief.[6] A rudimentary implementation into MCNP followed shortly

thereafter.[7] With an enhancement of the user interface and the addition of second order effects, this implementation has evolved into a standard MCNP feature.

II. VERIFICATION RESULTS

The perturbation results presented in this paper involve ten test problems taken from the MCNP 4A test suite. This initial verification effort differs from a benchmark in that experimental results are not available for comparison. The primary purpose of this effort is to verify the implementation of the differential operator perturbation technique in MCNP. To this end, this test suite includes several neutron, photon, and coupled fixed-source problems and two criticality problems. The intermediate 4XP version of MCNP was used to generate these perturbation results.

In each of these test problems, four perturbations were investigated, corresponding to approximately 5%, 10%, 20%, and 30% changes in a relevant tally. The 30% upper bound was chosen to verify the relevance and range of applicability of the second order term. The 5% lower bound was chosen to limit the execution time needed to determine the tally changes based on separate runs. Except where noted, a relevant tally was identified from among the existing tallies in the original input file. The tally results reported in this section are generally that for the total bin.

Five perturbation input files were generated for each test problem. In the first, the original input file was modified to include four PERT cards, one for each perturbation as discussed above. This input file produced the predicted change in the relevant tally for each of the four PERT cards. In each of the remaining four input files, the original input file was modified to include the actual perturbation prescribed on the corresponding PERT card. These files produced the actual change in the relevant tally.

Derivation of the perturbation equations implemented in MCNP, a description of the PERT card format, and a listing of the perturbation input files are given in Reference [8].

A. Test Problem Descriptions

This section provides a short description of each test problem included in this verification effort. The perturbation test suite is comprised of five neutron fixed-source problems (INP01, INP02, INP07, INP12, and INP14), one photon fixed-source problem (INP04), two coupled neutron/photon fixed-source problems (INP10 and INP11), and two criticality problems (INP09 and INP18).

1. Test Problem INP01. Input file INP01 consists of an inner sphere of graphite surrounded by a spherical shell of copper. There is an isotropic point source at the center of the graphite sphere with a uniform energy spectrum from 1 to 14.1 MeV. Tally 1 calculates the relative neutron current across the surface of the graphite sphere (adjusted by energy and cosine multipliers) and was chosen as the tally of interest for this problem. Results for the last cosine bin and total energy bin are reported below. The density of the graphite was reduced from 2.25 g/cm^3 to 1.85, 1.40, 0.60, and .005 g/cm^3, the latter of which increased Tally 1 by nearly 30%.

2. Test Problem INP02. Input file INP02 involves a simple geometric model consisting only of spheres. The large set of spheres include an inner region of boron surrounded by an aluminum shell. Within this aluminum shell, is another set of spheres filled with aluminum. The source is distributed

within the boron sphere and has a uniform energy spectrum from 0.1 to 1.0 MeV. The input file used for this test problem was further modified to disable the DXTRAN feature. Tally 1, which calculates the current across the boron-aluminum interface, was chosen as the tally of interest for this problem. The boron composition was perturbed from a ^{10}B atom fraction of .196 to a value of .250, .325, .510, and .720.

3. Test Problem INP07. Input file INP07 consists of a cylinder of UO_2 topped with a cylindrical plug of aluminum and enclosed in a large cylinder of rust. The neutron source is distributed throughout the UO_2 region and ranges in energy from 1-7 MeV. Tally 7 calculates the fission energy deposited in the UO_2 region and was chosen as the tally of interest for this problem. The UO_2 density was perturbed from 8.1 g/cm^3 to 8.8, 9.2, 10.3, and 11.5 g/cm^3.

4. Test Problem INP12. Input file INP12 involves a much more complex geometric model. This model includes an oil-well logging tool positioned in a borehole within a limestone formation. The tool consists of an americium/beryllium neutron source and two helium detectors embedded within a cylindrical region of iron. Water fills the cylindrical borehole between the tool and formation. The neutron source is directed radially into the limestone and ranges in energy from a few keV to 11 MeV. Taliy 44, which gives the absorption rate in the far detector, was chosen as the tally of interest for this problem. The iron density of the tool was decreased from 7.86 g/cm^3 to 7.72, 7.48, 7.17, and 6.84 g/cm^3.

5. Test Problem INP14. Input file INP14 consists of five repeated units within a sphere of carbon. Each of these five cubes is filled with ^{235}U and three rod containers. Each rod container includes four ^{235}U rods surrounded by carbon. A neutron source is distributed uniformly in each of the ^{235}U rods with an energy range of 1-11 MeV. The first tally bin of Tally 4 calculates the neutron flux averaged over the first ^{235}U rod in each of the 15 rod containers and was chosen as the tally of interest for this problem. The carbon density, within both the rod containers and the large sphere, was increased from 0.5 g/cm^3 to 1.0, 1.7, 3.5, and 6.0 g/cm^3.

6. Test Problem INP04. Input file INP04 consists of three sets of concentric spheres. The inner sphere of the largest set is filled with UH_3, while the outer spherical shell is filled with ULi_3. The smaller sets of spheres are contained within the outer spherical shell of the largest set. Both the inner and outer layers of these smaller spheres are filled with ULi_3. A 3 MeV point source is located at the center of the largest set of spheres. The input file used for this test problem was further modified to disable the DXTRAN feature. Tally 6, which gives the energy deposition in several materials, was chosen as the tally of interest for this problem. Results for cell 1 (UH_3) and the total energy bin are reported below. The UH_3 atom density was increased from 0.02 atoms/barn-cm to 0.0235, 0.0270, 0.035, and 0.04 atoms/barn-cm.

7. Test Problem INP10. Input file INP10 consists of two infinite concentric cylinders, where the inner cylinder is filled with water and the outer cylindrical shell is filled with copper. Near the origin, the inner cylindrical region is cut axially into seven cylindrical disks which are filled with water, carbon, void, water, carbon, water, and water, respectively. The void disk at the center contains a cube of CuO, and the water disk next to it contains a large void torus surrounded by a shell of copper. A neutron source is distributed uniformly in the cube of CuO and has an energy distribution given by the Watt fission spectrum. The last tally bin of Tally 4 gives the neutron flux averaged over the last segment of the right carbon disk and was chosen as the neutron tally of interest for this problem. A second tally of interest, Tally 14, gives the photon flux averaged over this same region. The copper density, surrounding both the infinite cylinder and the torus, was decreased from 8.94 g/cm^3 to 7.9, 6.9, 3.5, and 1.0 g/cm^3.

8. Test Problem INP11. Input file INP11 includes of a complex geometry with many odd shapes. A pretzel-shaped set of three tori filled with ^{235}U is centered at the origin. Traversing through these tori is a cage made of ellipsoids filled with SiO_2. Four "toys" of unique shape are arranged around the perimeter, each made of copper. All these objects are encased in a sphere of water. A disk-shaped, monodirectional neutron source is located in front of the tori within the water. The source energy distribution is uniform from .01 eV to 1 keV. The first tally bin of Tally 4 gives the neutron flux averaged over the three tori and was chosen as the neutron tally of interest for this problem. A second tally of interest, Tally 11, gives the photon current across the tori surfaces. The ^{235}U density within the three tori was increased from 7.8 g/cm^3 to 8.75, 9.5, 10.9, and 12.0 g/cm^3.

9. Test Problem INP09. Input file INP09 consists of a 10 cm cube filled with ^{235}U. Two rectangular pieces of copper are implanted in this cube, and a cone-shaped hole extends from one side into the center. A second cone-shaped region of ^{235}U protrudes from another side of the cube. The cube is surrounded by a sphere of air (20 cm radius). This problem was executed in criticality mode and had a final combined k_{eff} of 1.0133 $\pm$ .00015. Tally 14, a track-length estimate of k_{eff}, was added to this problem to estimate the effect of the perturbation on the eigenvalue. The surrounding air density was increased from 0.01 g/cm^3 to 0.49, 0.90, 2.0, and 3.0 g/cm^3.

10. Test Problem INP18. Input file INP18 includes a triangular pitched nuclear reactor core. The hexagonal lattice of fuel rods is contained within a cylindrical core. Five whole and three partial control rods, filled with a mixture of boron and carbon, are included in the core. The fuel rods are 70% enriched uranium, and the clad on the fuel is a mixture of zirconium and niobium with a inner liner of tungsten. Inside the clad, the fuel is cooled by a water blanket. Water is also used as the moderator and heat transfer agent between the fuel rods. The water is a mixture of heavy and light water. When executed in criticality mode, this problem produced a final combined k_{eff} of 1.0379 $\pm$ .0002. Again Tally 14 was added to this input file to produce a track-length estimate of k_{eff}. The water density was increased from 1.0 g/cm^3 to 1.5, 2.3, 4.0, and 6.0 g/cm^3.

B. First Order Versus Second Order

This section discusses the relevance and range of applicability of the first and second order terms of the Taylor series expansion. Clearly if a response is a linear function of a perturbed parameter, the first order estimator will accurately predict any size of change in that response - likewise for a response that exhibits a quadratic behavior and a second order estimator is added. However, as demonstrated in the following perturbation results, this is rarely the case over the range of interest. Figure 1 presents the perturbation results for test problem INP02 with the first order estimator separated from the default estimator (first plus second order). In this case, the second order term clearly makes a significant contribution to predicted changes in the response that exceed 10%.

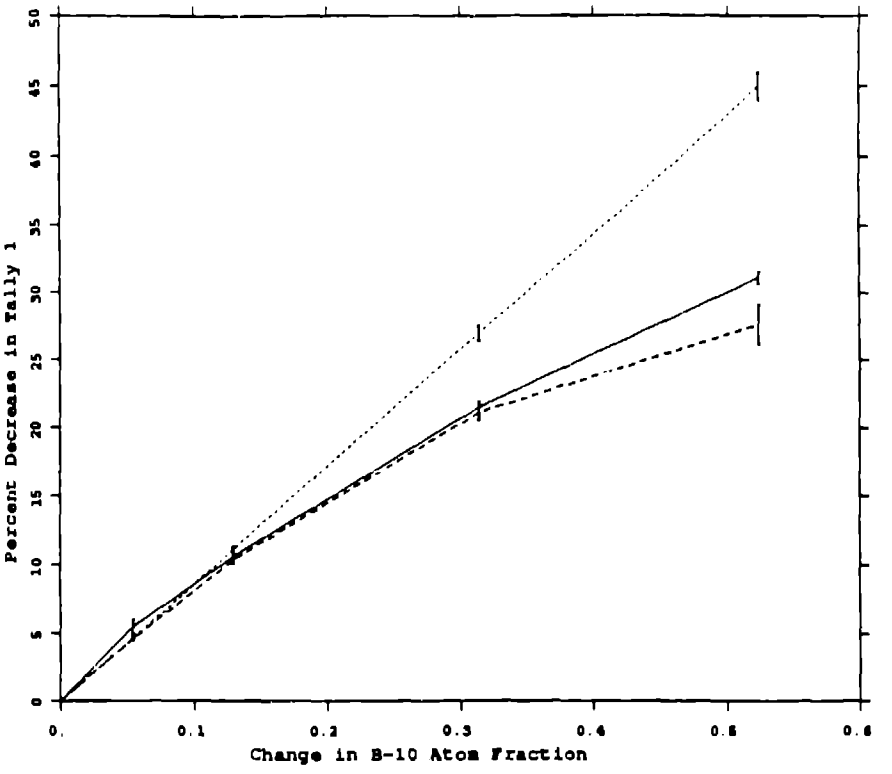

Fig. 1. Change in Tally 1 of problem INP02 due to an increase in the ^{10}B atom fraction. Solid line gives the actual change; dashed line gives the first and second order predicted change; dotted line gives the first order predicted change.

Analyzing the first and second order perturbation results leads to the following rules of thumb. The first order perturbation estimator typically provides sufficient accuracy for response changes that are less than 5%. The default first and second order estimator offers acceptable accuracy for response changes that are less than 20-30%. This upper bound depends on the behavior of the response as a function of the perturbed parameter. The magnitude of the second order estimator is a good measure of the range of applicability. If this magnitude exceeds 30% of the first order estimator, it is likely that higher order terms are needed for an accurate prediction. The METHOD keyword on the PERT card allows one to tally the second order term separate from the first. The following PERT cards demonstrate this:

```
PERT1:n cell=1 rho=-3.5
PERT2:n cell=1 rho=-3.5 method=2
PERT3:n cell=1 rho=-3.5 method=3
```

The first PERT card generates the default (first plus second order) perturbation results; the second produces only first order results; and the third gives only second order results. Once the behavior of a perturbation is understood, unneeded PERT cards can be removed from future analyses.

C. Test Problem Results

Table I gives the actual and predicted percent changes in the tally of interest for each test problem. The relative error associated with each change is given in parentheses. The "Actual" differential change was obtained by subtracting the actual perturbed and unperturbed results; whereas, the predicted change, produced by the PERT card, gives the differential change directly. These differential changes were normalized by the unperturbed tally to give the percent change.

The "DIFF" column in Table I gives the difference between the actual and predicted results. In general, the accuracy of the differential operator technique appears to be within a couple percent for up to 20-30% changes in a response. Exceptions to this include test problems INP09 and INP10. The most likely explanation for the deviation of test problem INP09 is that this technique does not currently account for perturbations in the shape of the eigenfunction. The deviation shown for the photon tally of test problem INP10 is due to the higher order behavior of the response perturbation which cannot be accurately estimated by first and second order terms of the Taylor series expansion.

TABLE I
SUMMARY OF MCNP PERTURBATION RESULTS

Test Problem	First Perturbation ~5%			Second Perturbation ~10%			Third Perturbation ~20%			Fourth Perturbation ~30%		
	Actual	PERT	Diff	Actual	PERT	Diff	Actual	PERT	Diff	Actual	PERT	Diff
Neutron Fixed-Source												
INP01	5.02% (.0695)	4.75% (.0061)	-0.27%	10.38% (.0341)	10.28% (.0064)	-0.10%	20.36% (.0176)	20.59% (.0071)	0.23%	28.58% (.0129)	28.65% (.0076)	0.07%
INP02	-5.47% (.0924)	-4.59% (.0193)	0.88%	-10.56% (.0469)	-10.32% (.0189)	0.24%	-21.46% (.0221)	-21.11% (.0268)	0.35%	-31.15% (.0146)	-27.65% (.0532)	3.50%
INP07	5.27% (.1887)	5.83% (.0351)	0.56%	9.77% (.1102)	9.31% (.0365)	-0.46%	20.62% (.0556)	19.47% (.0402)	-1.15%	33.98% (.0381)	31.52% (.0443)	-2.46%
INP12	5.88% (.1924)	3.54% (.0088)	-2.34%	10.45% (.1103)	9.97% (.0090)	-0.48%	20.91% (.0586)	18.91% (.0093)	-2.00%	30.19% (.0418)	29.24% (.0095)	-0.95%
INP14	4.46% (.2840)	3.50% (.0117)	-0.96%	10.54% (.1293)	8.63% (.0191)	-1.91%	20.30% (.0712)	23.16% (.0380)	2.86%	30.13% (.0523)	46.45% (.0608)	16.32%
Photon Fixed-Source												
INP04	-4.69% (.0635)	-4.73% (.0158)	0.04%	-9.17% (.0331)	-9.30% (.0144)	0.13%	-18.52% (.0168)	-19.09% (.0128)	0.57%	-23.62% (.0135)	-24.75% (.0134)	1.13%
Coupled Neutron/Photon Fixed-Source												
INP10 Neutron	4.82% (.2094)	3.99% (.0268)	-0.83%	7.80% (.1288)	7.79% (.0305)	-0.01%	20.43% (.0522)	20.45% (.0496)	0.02%	28.09% (.0385)	29.51% (.0666)	1.42%
INP10 Photon	5.82% (.1606)	6.04% (.0217)	0.22%	11.51% (.0833)	12.13% (.0244)	0.62%	28.10% (.0357)	34.97% (.0381)	6.87%	4.41% (.1939)	53.84% (.0488)	49.43%
INP11 Neutron	5.82% (.2900)	5.45% (.0120)	-0.37%	10.83% (.1651)	10.25% (.0126)	-0.58%	22.68% (.0925)	20.40% (.0140)	-2.28%	30.81% (.0764)	29.44% (.0151)	-2.37%
INP11 Photon	1.37% (1.0989)	1.49% (.0313)	0.12%	1.92% (.7944)	3.09% (.0290)	1.17%	7.97% (.2047)	7.03% (.0273)	-0.94%	9.56% (.1778)	11.02% (.0269)	1.46%

TABLE I
SUMMARY OF MCNP PERTURBATION RESULTS

Test Problem	First Perturbation ~5%			Second Perturbation ~10%			Third Perturbation ~20%			Fourth Perturbation ~30%		
	Actual	PERT	Diff	Actual	PERT	Diff	Actual	PERT	Diff	Actual	PERT	Diff
Criticality												
INP09	5.13% (.0288)	6.69% (.0197)	1.56%	9.62% (.0160)	12.31% (.0355)	2.69%	20.35% (.0089)	27.01% (.0797)	6.66%	29.13% (.0067)	39.87% (.1216)	10.74%
INP18	4.49% (.0378)	4.83% (.0097)	0.34%	10.46% (.0192)	11.00% (.0168)	0.54%	20.80% (.0117)	19.68% (.0429)	-1.12%	30.02% (.0092)	21.60% (.1053)	-8.42%

III. SUMMARY

Results presented in this paper verify the applicability of the differential operator perturbation technique as implemented within MCNP. This capability is shown to be relevant for fixed-source problems (neutron, photon, and coupled neutron/photon) as well as criticality applications. Furthermore, this technique can be used to estimate the effects of multiple perturbations in a single run with minimal loss (5-10% per perturbation) of performance. A key advantage of this method is that the precision of the estimator remains bounded, even as the magnitude of the perturbation vanishes.

In general, the accuracy of the differential operator technique appears to be within a couple percent for up to 20-30% changes in a response. For small response perturbations (< 5%), it was found that use of only the first order estimator typically offers sufficient accuracy.

Possible enhancements to the MCNP perturbation feature include compatibility with point detectors, DXTRAN spheres, k_{eff} estimators, and electron transport. While application of the differential operator technique to the first three areas is fairly straightforward, its application to electron transport has not yet been investigated. Future effort related to the perturbation feature will also include additional verification work, with an emphasis on experimental applications.

REFERENCES

1. J. Briesmeister, Editor, "MCNP — A General Monte Carlo N-Particle Transport Code," LA-12625-M, Los Alamos National Laboratory (1993).

2. J. E. Olhoeft, "The Doppler Effect for a Non-Uniform Temperature Distribution in Reactor Fuel Elements," WCAP-2048, Westinghouse Electric Corporation, Atomic Power Division, Pittsburgh (1962).

3. H. Takahashi, "Monte Carlo Method for Geometrical Perturbation and its Application to the Pulsed Fast Reactor," Nucl. Sci. Eng. **41**, p. 259 (1970).

4. M. C. Hall, "Monte Carlo Perturbation Theory in Neutron Transport Calculations," Ph. D. Thesis,

University of London (1980).

5. M. C. Hall, "Cross-Section Adjustment with Monte Carlo Sensitivities: Application to the Winfrith Iron Benchmark," Nucl. Sci. Eng. **81**, p. 423 (1982).

6. H. Rief, "Generalized Monte Carlo Perturbation Algorithms for Correlated Sampling and a Second-Order Taylor Series Approach," Ann. Nucl. Energy **11**, p. 455 (1984).

7. G. McKinney, "A Monte Carlo (MCNP) Sensitivity Code Development and Application," M.S. Thesis, University of Washington (1984).

8. G. W. McKinney and J. L. Iverson, "Verification of the Monte Carlo Differential Operator Technique for MCNP," LA-13098, Los Alamos National Laboratory (1996).